

Cite this: DOI: 00.0000/xxxxxxxxxx

Received Date

Accepted Date

DOI: 00.0000/xxxxxxxxxx

Consistent GMTKN55 and molecular-crystal accuracy using minimally empirical DFT with XDM(Z) dispersion[†]

Kyle R. Bryenton^a and Erin R. Johnson^{a,b,*}

Density-functional theory (DFT) has become the workhorse of modern computational chemistry, with dispersion corrections such as the exchange-hole dipole moment (XDM) model playing a key role in high-accuracy modelling of large-scale systems. All previous production implementations of XDM have used the two-parameter Becke–Johnson damping function based on atomic radii. Here, we introduce and implement a new XDM variant that uses a one-parameter damping function based on atomic numbers, recently proposed by Becke. Both this new Z damping and the canonical BJ-damping variants of XDM are benchmarked on the comprehensive GMTKN55 database using minimally empirical generalised-gradient-approximation, global hybrid, and range-separated hybrid functionals. This marks the first time that the XDM (and many-body dispersion, MBD) corrections have been tested on the GMTKN55 set. Using the new WTMAD-4 metric, an outlier analysis is performed for all new data, as well as for top-ranking functionals from the literature at each rung, providing insight into both performance and consistency across the dataset. To test Z damping's transferability to the solid state, four benchmarks involving molecular crystals are also considered. Across these molecular and solid-state benchmarks, the revPBE0 and B86bPBE0 hybrid functionals, paired with the Z damped XDM variant, show excellent performance.

1 Introduction

Despite being the weakest of the van der Waals forces, London dispersion interactions are collectively extremely important in determining the structural and energetic properties of many chemical systems. Because dispersion physics is not included in most density-functional approximations (DFAs) for modelling electronic structure, they are commonly augmented by a dispersion correction (DC). Numerous such dispersion methods exist in the literature and may be divided into two classes: (i) explicitly non-local corrections that are included within the self-consistent field (SCF) procedure, and (ii) additive, post-SCF corrections. The first type includes the family of van der Waals functionals (vdW-DF),^{1–3} as well as (r)VV10.^{4,5} However, due to their non-local nature, these methods are significantly more expensive than additive corrections. Popular post-SCF methods include the Grimme-D series (D1,⁶ D2,⁷ D3(0),⁸ D3(BJ),⁹ D4¹⁰); the many-body dispersion family (TS,¹¹ MBD@rsSCS,^{12,13} MBD-NL¹⁴

uMBD,¹⁵ MBD-FI¹⁶); and the exchange-hole dipole moment (XDM) model.¹⁷

XDM was originally formulated between 2005 and 2007^{18–20} and has since proven to be one of the most broadly accurate DFA dispersion treatments due to its limited empiricism and inclusion of important physical considerations.^{21,22} XDM has demonstrated accuracy, efficiency, and stability in modelling dispersion binding across a highly diverse range of chemical systems, including intermolecular complexes,^{23,24} bulk metals,²⁵ salts,^{26,27} layered materials,²⁸ surfaces,^{29,30} and molecular crystals.^{31,32} The recent implementation of XDM in the FHI-aims³³ software, and pairing with hybrid functionals, allows computation of molecular crystal lattice energies with the highest accuracy of any dispersion-corrected DFT reported to date.³⁴ It has also shown great success in the area of molecular crystal structure prediction (CSP).^{35,36}

However, Becke recently showed³⁷ that XDM fails to accurately predict the binding energies of two alkali-metal clusters (Li_8 and Na_8) in the ALK8 subset of the GMTKN55 thermochemistry benchmark.³⁸ The error was traced to the Becke–Johnson (BJ) damping function¹⁹ used in XDM to damp the dispersion energy to a small negative value at short interatomic separations. An alternative damping function based on atomic numbers, Z , was proposed and found to provide good accuracy for these metal clusters, and the GMTKN55 benchmark as a whole.³⁷ Notably, the Z -dependent damping function is simpler, relying on only one empirical parameter for use with a given DFA, as opposed

^a Department of Physics and Atmospheric Science, Dalhousie University, 6310 Coburg Road, Halifax, Nova Scotia, Canada, B3H 4R2

^b Department of Chemistry, Dalhousie University, 6243 Alumni Crescent, Halifax, Nova Scotia, B3H 4R2, Canada. E-mail: erin.johnson@dal.ca

^c Yusuf Hamied Department of Chemistry, University of Cambridge, Lensfield Road, Cambridge, CB2 1EW, United Kingdom.

[†] Electronic Supplementary Information (ESI) available, see DOI: 10.1039/cXCP00000x/

to the two parameters used in BJ damping. However, the performance of Z damping has not yet been assessed on solid-state systems, or in conjunction with any other density functionals beyond the DH24 double hybrid. For the present study, Z damping was implemented in the FHI-aims code, and the performance of BJ- and Z-damped variants of XDM, paired with an assortment of minimally empirical density functionals, is assessed for the GMTKN55 and selected molecular-crystal benchmarks. Further, the Z-damping function has been implemented for the open-source code, PostG,^{23,39} which allows the XDM(Z) dispersion correction to be applied *ad hoc* to any of the dozens of quantum-chemical codes that write .wfx, .wfn, or .molden files.*

2 Theory

The XDM dispersion energy is written as a sum over all pairs of atoms, i and j :

$$E_{\text{disp}}^{\text{XDM}} = - \sum_{i < j} \left(\frac{C_{6,ij} f_6}{R_{ij}^6} + \frac{C_{8,ij} f_8}{R_{ij}^8} + \frac{C_{10,ij} f_{10}}{R_{ij}^{10}} \right). \quad (1)$$

Here, C_n dispersion coefficients are computed for each atom pair from the self-consistent electron density of the system, as well as the density gradient, Laplacian, kinetic-energy density, and Hirshfeld atomic partitioning weights. The f_n damping functions depend on the interatomic distance, R_{ij} , and will be discussed in detail in the remainder of this section.

Conventionally, XDM uses the Becke–Johnson (BJ) damping function,¹⁹ which is also used in the D3(BJ) and D4 dispersion methods of Grimme and co-workers. This damping function is given by

$$f_n^{\text{BJ}}(R_{ij}) = \frac{R_{ij}^n}{R_{ij}^n + R_{\text{vdW},ij}^n}, \quad (2)$$

where $R_{\text{vdW},ij}$ is the sum of approximate van der Waals radii of atoms i and j . It is determined as

$$R_{\text{vdW},ij} = a_1 R_{c,ij} + a_2, \quad (3)$$

where a_1 and a_2 are empirical parameters that are not element-dependent but are fitted for use with a particular combination of density functional and basis set. $R_{c,ij}$ is a “critical” interatomic distance at which successive terms in the perturbation theory expansion of the dispersion energy become equal. If the dispersion energy only includes the C_6 and C_8 terms, then

$$R_{c,ij} = \sqrt{\frac{C_{8,ij}}{C_{6,ij}}}. \quad (4)$$

However, if the C_{10} term is also included in the dispersion energy, two other possible definitions for $R_{c,ij}$ arise:

$$R_{c,ij} = \begin{cases} \sqrt{\frac{C_{10,ij}}{C_{8,ij}}} \\ \sqrt[4]{\frac{C_{10,ij}}{C_{6,ij}}} \end{cases}. \quad (5)$$

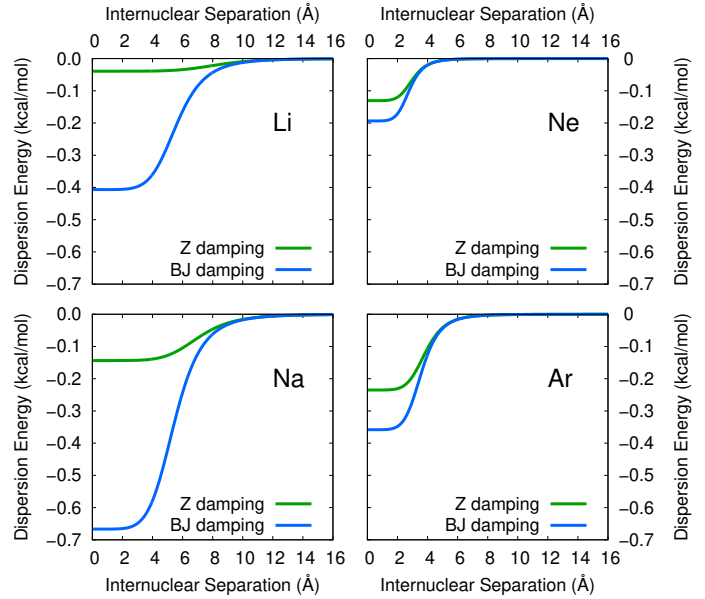


Fig. 1 Comparison of BJ- and Z-damping functions. The plots use XDM data for the free atoms only, computed with the B86bPBE functional and tight basis settings using FHI-aims.

In XDM, the value of $R_{c,ij}$ is taken to be the average of these three results:

$$R_{c,ij} = \frac{1}{3} \left[\left(\frac{C_{8,ij}}{C_{6,ij}} \right)^{1/2} + \left(\frac{C_{10,ij}}{C_{6,ij}} \right)^{1/4} + \left(\frac{C_{10,ij}}{C_{8,ij}} \right)^{1/2} \right]. \quad (6)$$

Becke recently proposed an alternative damping function for use with XDM that, unlike BJ damping, involves only one empirical fit parameter.³⁷ In this work, it will be referred to as Z damping, due to the dependence on the atomic number. The Z-damping function is

$$f_n^Z(R_{ij}) = \frac{R_{ij}^n}{R_{ij}^n + z_{\text{damp}} \frac{C_{n,ij}}{Z_i + Z_j}}, \quad (7)$$

where Z_i and Z_j are the atomic numbers of atoms i and j , respectively. This definition was chosen because the resulting contribution to the correlation energy in the united-atom limit would be

$$\lim_{R_{ij} \rightarrow 0} \left(\frac{C_{n,ij}}{R_{ij}^n + z_{\text{damp}} \frac{C_{n,ij}}{Z_i + Z_j}} \right) = \frac{Z_i + Z_j}{z_{\text{damp}}}, \quad (8)$$

and atomic correlation energies are roughly proportional to atomic number. Similar to BJ damping, the single empirical parameter, z_{damp} , is atom-independent and fitted for use with a particular density functional and basis set. A typical value of z_{damp} is around 10^5 Ha^{-1} .

To illustrate the differences in damping functions, BJ and Z damping are compared for homonuclear interactions between Li, Na, Ne, and Ar atoms in Figure 1. The Li and Na calculations are spin-polarized, with a net spin of 1 electron. For simplicity, the curves use only data for the free atoms, which omit changes in dispersion coefficients with internuclear separation that would be observed in the dimer systems due to varying electron densities. The results in Figure 1 show that Z damping consistently reduces

* Since many dialects of the .molden filetype exist, users must verify the input file is handled correctly.

the magnitude of the dispersion energy compared to BJ damping. However, this effect is fairly minor for Ne and Ar, while there is a very large increase in damping strength for Li and Na. This allows correction of the overbinding seen with BJ damping for the Li₂ and Na₂ clusters, while preserving high accuracy for main-group elements. With BJ damping, the magnitudes of the dispersion energies in the united-atom limit follow the trend Na>Li>Ar>Ne, but this changes to Ar>Na≈Ne>Li for Z damping. The latter appears more physical because, in the united-atom limit, the dispersion energy would become a correlation energy and should increase with the number of electrons and, hence, atomic number.

3 Data Sets

To evaluate the performance of XDM with both BJ and Z damping, a comprehensive list of benchmarks has been selected for testing. These are categorised into three groups: those used to optimize parameters for damping functions, finite-molecule benchmarks, and molecular-crystal benchmarks. The benchmark content, geometry sources, and reference data quality are summarised below.

3.1 Damping-Parameter Fit Set

KB49: Binding energies of 49 molecular dimers with reference values from basis-set extrapolated CCSD(T) calculations.⁴⁰ Dimer geometries are available from the [refdata](#) GitHub repository.⁴¹ The BJ-damping parameters, a_1 and a_2 (in Å), as well as the Z-damping parameter, z_{damp} , were fitted separately for each combination of DFA and basis set. Optimal parameters were determined by minimising the root-mean-square percent error (RM-SPE) for the KB49 set.

3.2 Molecular Benchmarks

GMTKN55: A collection of 55 individual benchmarks spanning the thermochemistry of small and large molecules, reaction barriers, and both intramolecular and intermolecular non-covalent interactions. Ref. 38 provides detailed information regarding the individual benchmarks. Geometries for FHI-aims may be obtained from the [gmtkn55-fhiaims](#) GitHub repository.⁴²

Due to the wide range of energy scales of the component benchmarks within the GMTKN55, the overall error for the set is reported as a weighted mean absolute deviation (WTMAD). While several definitions for such a weighted error have been proposed, we focus on our recent WTMAD-4 in this work. In this scheme, each subset is assigned a weight, denoted w_i , based on the mean error ($\overline{\text{MAD}}_i$) obtained from a set of 10 representative minimally empirical hybrid functionals:⁴³

$$w_i = \frac{100}{N_{\text{bench}}} \left(\frac{3.5}{\overline{\text{MAD}}_i^{\text{10-DFA}}} \right). \quad (9)$$

The specific values of the weights are given in the ESI. The WTMAD-4 for a given dispersion-corrected functional is then calculated as

$$\text{WTMAD-4} = \frac{1}{N_{\text{bench}}} \sum_{i=1}^{N_{\text{bench}}} w_i \cdot \text{MAD}_i. \quad (10)$$

See Ref. 43 for the specific set of 10 functionals used to evaluate the weights and more information regarding the formulation of the WTMAD-4.

In this work, we also report the number, $N_{r>h}$, of benchmarks that have a ratio of $\text{MAD}_i / \overline{\text{MAD}}_i^{\text{10-DFA}} > h$, where the mean MAD is the value obtained from the 10 reference DFAs used in the definition of the WTMAD-4 weights. Similarly, $N_{d>h}$ is the number of benchmarks that have the difference $\text{MAD}_i - \overline{\text{MAD}}_i^{\text{10-DFA}} > h$ in units of kcal/mol. We would ideally want $N_{r\leq 1} = N_{d\leq 0}$ to be 55, meaning equal or better performance than the average of the chosen 10 functionals for all of the benchmarks, but barring that, we seek to avoid any extreme outliers in terms of both absolute and percent errors by minimising both $N_{d>2}$ and $N_{r>2}$. These criteria, qualitatively, identify cases where the error more than doubles relative to the 10-DFA mean, or exceeds it by more than 2 kcal/mol.

3.3 Solid-State Benchmarks

X23: Lattice energies of 23 molecular crystals,^{31,44} using updated “X23b” reference energies.⁴⁵ Geometries are available from the [refdata](#) repository.⁴¹ Unlike the previous benchmarks, X23 requires geometry optimisations with each functional and basis combination considered.

HalCrys4: Lattice energies of four halogen crystals—Cl₂, Br₂, I₂, and ICl.⁴⁶ The lattice energies are compared to back-corrected experimental results from Ref. 47. As with the X23, geometries are optimised for each reported functional and basis set. Geometries are available from the [refdata](#) repository.⁴¹

ICE13: Absolute lattice energies of ice polymorphs⁴⁸ (Abs), along with their relative energy differences (Rel) using diffusion Monte Carlo (DMC) reference data.⁴⁹ ICE13 requires geometry optimisations for all systems except the isolated water molecule, which uses a fixed geometry. Geometries are available from the [refdata](#) repository.⁴¹

4 Computational Methods

All calculations were performed using versions 250425 or 250711 of FHI-aims.^{33,34,50–55} As noted above, the BJ- and Z-damping coefficients were determined for each functional and basis combination by least-squares fitting to minimise the RMSPE for the KB49 benchmark set of intermolecular binding energies. Parameters for the XDM(BJ) and XDM(Z) dispersion corrections, optimised for all combinations of 16 density functionals and five basis sets, are included in the ESI. An updated list of all XDM BJ- and Z-damping parameters for various functional–basis combinations is kept in the [refdata](#) GitHub repository.⁴¹ For a version of FHI-aims that automatically sets the XDM damping parameters for all functionals considered here, the interested reader is directed to versions 260110 onwards.

At the GGA level of theory, we considered the PBE,^{56–58} revPBE,⁵⁹ and B86bPBE⁶⁰ functionals. At the global hybrid level, we selected several GGA-based hybrids including B3LYP,^{61–65} popular for molecular thermochemistry; PBE0,⁶⁶ popular in solid-state chemistry; revPBE0,^{59,66} popular for studies of water; and our previously recommended B86bPBE0.³⁴ We also used the analogues of these functionals with 50% exact exchange (BH-

LYP⁶⁷, PBE50, revPBE50, and B86bPBE50), which should exhibit reduced delocalisation error.⁶⁸ Finally, we considered the range-separated GGA-based hybrid, HSE06,⁶⁹ and four parameterisations of the LC- ω (h)PBE functional.^{70,71}

It is notable that the TS,¹¹ MBD@rsSCS,¹³ and MBD-NL¹⁴ dispersion corrections, also available in FHI-aims, have not been tested for the GMTKN55 benchmark. As a result, calculations were performed using each of these three dispersion corrections, paired with only the PBE and PBE0 functionals due to the limited availability of damping parameters. Additionally, while D3(BJ) has been widely applied in the literature,³⁸ the MAE data is not available for its pairing with revPBE0 specifically, which is found to be one of the top-performing hybrids.⁷² Thus, D3(BJ) calculations were performed for the PBE, PBE0, revPBE, and revPBE0 functionals using FHI-aims. This allows comparison between FHI-aims (this work) and Gaussian-basis (Ref. 38) results for the other three functionals.

For GMTKN55, all FHI-aims calculations used the `tight` basis, except for subsets containing anions. HB21, BH76, BH76RC, and G21EA used `tier2_aug2` for all atoms; IL16 used `tier2_aug2` for all O, F, S, and Cl atoms; and WATER27 used `tier2_aug2` for O atoms only for reactions involving anions, as this basis caused linear dependencies in the SCF for some of the larger, neutral water clusters. In all cases, the damping parameters were kept at the same values optimised for the `tight` basis settings as these are already sufficiently converged as to approach the basis-set limit.

Turning to the solid-state, only the three GGA and six global-hybrid functionals were considered (B3LYP and BLYP were omitted as the asymptotic constraint used in the construction of the B88 exchange functional⁶¹ is not relevant for solid-state systems). The GGA calculations used both the `tight` and `lightdenser` basis settings as the latter is our recommended basis for most solid-state calculations (particularly geometry optimisations), although there will be some residual basis-set incompleteness error. For the hybrid functionals, only `lightdenser` calculations were performed as calculations with the `tight` basis require prohibitive amounts of memory. Hybrid results with the `tight` basis were approximated using an additive basis set correction evaluated at the converged GGA/`lightdenser` geometries:^{34,73}

$$\begin{aligned} E(\text{hybrid/tight}) \approx & E(\text{hybrid/lightdenser}) \\ & + E(\text{GGA/tight}) \\ & - E(\text{GGA/lightdenser}). \end{aligned} \quad (11)$$

As previously mentioned, this work employs the new `lightdenser` basis, which builds on the `lightdense` basis introduced in Ref. 34 and is now packaged in the species defaults of the FHI-aims code. `lightdense` uses `light` basis functions and increases the integration grids to those of the `tight` basis defaults, removing instabilities that resulted in artificial minima in the potential energy surface and could sometimes prevent convergence of geometry optimisations to their true minima. The `lightdenser` basis builds on this by also increasing the Hartree potential (`l_hartree`) to 8, resolving a small force–energy in-

Table 1 Timing comparisons for XDM are reported as the mean of the percent van der Waals (vdW) time per system. For the “1 SCF Step” column, each GMTKN55 system was reinitialized from a converged SCF using the `elsi_restart` feature, and was allowed to converge—typically one SCF step—using the B86bPBE0 hybrid functional and `tight` basis settings. For the “1 Opt Step” column, each system in the X23 benchmark was started from a pre-converged geometry, thus a single geometry optimisation step was calculated. The results combine data from PBE, B86bPBE, and their associated 25% and 50% hybrid functionals, all using the `lightdenser` basis.

Method	1 SCF Step	1 Opt Step
XDM(BJ)	9.42%	3.20%
XDM(Z)	9.16%	3.20%

consistency that could, on rare occasions, also prevent convergence of geometry optimisations. This `lightdenser` basis offers increased stability while incurring only slightly more computation time and a negligible increase in memory requirements compared to its `light` counterpart. We recommend this `lightdenser` basis, particularly for solid-state applications or in cases where the `tight` basis is prohibitively large.

Lastly, we highlight the computational efficiency of the XDM-based post-SCF dispersion corrections. As shown in Table 1, these corrections account for only a small fraction of the total CPU time compared to even a single SCF step. Z damping is slightly quicker than BJ damping, although not enough to be significant during a geometry optimisation.

5 Results and Discussion

5.1 Molecular Benchmarks

The focus of this section is the GMTKN55 set, comprised of 55 diverse molecular benchmarks. Table 2 shows a detailed comparison of the performance of XDM(BJ) versus XDM(Z) for each of the component benchmarks using three selected DFAs. Full statistics for each benchmark with all functionals and dispersion corrections, as well as the WTMAD- N values for each category, are provided in the ESI.

From the results in Table 2, Z damping shows clear improvements for ALK8 (dissociation and other reactions of alkaline compounds), HEAVYSB11 (dissociation energies of heavy-element compounds), YBDE18 (bond-dissociation energies of ylides), and BSR36 (bond-separation reactions of saturated hydrocarbons). Conversely, BJ damping performs better for DARC (Diels-Alder reaction energies), NBPRC (oligomerisations, H₂ fragmentations, and H₂ activation reactions involving NH₃/BH₃ or PH₃/BH₃ systems), PA26 (adiabatic proton affinities), and RC21 (fragmentations and rearrangements in radical cations). For most other subsets, there is little to choose between the two damping schemes.

Comparing the three selected functionals, B86bPBE0 consistently achieves the minimum error on the MB16-43 (mindless benchmarking) subset, with MAEs of 13.7 and 14.0 kcal/mol; for comparison, it has been noted that “MADs for MB16-43 usually exceed 15 kcal/mol for most dispersion-corrected hybrid DFAs.”³⁸ In terms of outliers, LC- ω hPBE is conspicuously poor for C₆₀ISO (relative energies of C₆₀ isomers), while revPBE0 gives large errors for W4-11 (total atomisation energies), ALKBDE10

Table 2 Comparison of MADs (in kcal/mol) for the individual GMTKN55 benchmarks using the selected functionals with either XDM(BJ) or XDM(Z). Also shown for comparison are the $\overline{\text{MAD}}_i^{\text{10-DFA}}$ values from the 10 representative DFAs used in the definition of the WTMAD-4; these mean values are used to quantify outliers. Entries are shaded according to their difference from the $\overline{\text{MAD}}_i^{\text{10-DFA}}$ values.

	10-DFA		revPBE0		B86bPBE0		LC-whPBE	
	$\overline{\text{MAD}}_i$		BJ	Z	BJ	Z	BJ	Z
AL2X6	1.94	0.99	1.56	0.91	1.21	1.44	1.54	
ALK8	4.88	12.59	3.49	9.43	3.04	9.74	2.65	
ALKBDE10	6.03	7.34	7.35	5.33	5.36	5.07	5.10	
BH76RC	2.49	1.71	1.76	1.95	1.97	2.16	2.21	
DC13	8.16	8.84	8.85	7.94	8.01	9.20	9.48	
DIPCS10	3.86	3.15	3.40	3.24	3.33	2.83	2.86	
FH51	2.66	2.21	2.39	2.42	2.61	2.77	2.99	
G21EA	2.97	3.17	3.17	2.62	2.64	2.42	2.44	
G21IP	3.92	3.79	3.85	3.76	3.78	3.90	3.93	
G2RC	5.67	5.43	5.46	5.97	6.02	6.21	6.33	
HEAVYSB11	2.33	2.25	1.77	1.58	1.14	2.05	1.52	
NBPRC	2.74	1.75	2.20	2.28	2.62	2.89	3.28	
PA26	3.21	3.97	4.46	2.80	3.15	2.21	2.57	
RC21	4.40	4.20	4.64	4.74	5.11	5.12	5.51	
SIE4x4	13.60	13.98	14.03	14.10	14.17	12.82	12.90	
TAUT15	1.10	0.83	0.94	1.05	1.10	0.93	0.98	
W4-11	5.92	8.77	8.75	3.88	3.77	3.41	3.40	
YBDE18	2.50	2.66	2.06	1.67	1.36	1.06	0.93	
BSR36	3.14	1.84	0.78	3.18	2.44	1.92	1.29	
C60ISO	5.34	2.14	2.18	2.25	2.29	9.76	9.93	
CDIE20	1.11	1.10	0.94	1.21	1.13	0.77	0.71	
DARC	4.41	3.63	5.06	2.55	3.61	5.89	6.90	
ISO34	1.42	1.27	1.29	1.30	1.31	1.42	1.43	
ISOL24	3.19	1.76	2.26	1.99	1.99	3.19	3.60	
MB16-43	19.30	15.60	15.27	13.67	14.00	14.93	14.92	
PARel	1.16	0.98	1.07	1.07	1.11	1.00	1.05	
RSE43	1.21	1.00	0.70	1.34	1.17	1.16	1.00	
BH76	4.17	3.30	3.46	3.92	4.07	3.14	3.21	
BHDIV10	3.83	3.90	4.01	4.27	4.34	3.25	3.31	
BHPERI	2.78	3.21	3.16	2.63	2.81	2.11	2.28	
BHROT27	0.58	0.44	0.47	0.52	0.54	0.44	0.44	
INV24	1.44	0.97	0.98	1.02	1.02	1.15	1.17	
PX13	5.40	3.87	4.31	5.53	5.88	5.84	6.18	
WCPT18	3.59	2.80	3.12	3.62	3.86	3.65	3.88	
ADIM6	0.17	0.22	0.10	0.18	0.09	0.11	0.14	
AHB21	1.02	0.56	0.76	1.12	1.32	0.96	1.13	
CARBBH12	1.16	0.82	0.85	1.18	1.24	0.96	1.02	
CHB6	1.54	1.52	1.72	1.15	1.38	1.47	1.67	
HAL59	0.66	0.44	0.82	0.56	0.90	0.38	0.66	
HEAVY28	0.46	0.18	0.60	0.21	0.59	0.15	0.45	
IL16	0.55	0.56	0.55	0.34	0.76	0.32	0.61	
PNICO23	0.81	0.44	0.53	0.59	0.69	0.45	0.53	
RG18	0.21	0.09	0.14	0.05	0.09	0.04	0.10	
S22	0.47	0.24	0.25	0.38	0.44	0.30	0.35	
S66	0.35	0.18	0.19	0.29	0.33	0.24	0.30	
WATER27	4.44	1.51	1.11	4.51	6.12	4.28	6.01	
ACONF	0.10	0.19	0.08	0.04	0.04	0.09	0.10	
Amino20x4	0.28	0.26	0.29	0.25	0.27	0.25	0.28	
BUT14DIOL	0.21	0.14	0.15	0.30	0.33	0.31	0.34	
ICONF	0.32	0.25	0.31	0.27	0.28	0.27	0.32	
IDISP	2.54	1.08	1.25	1.69	1.51	2.32	2.44	
MCONF	0.30	0.24	0.23	0.22	0.24	0.27	0.33	
PCONF21	0.74	0.44	0.60	0.73	0.72	0.61	0.59	
SCONF	0.33	0.32	0.35	0.38	0.52	0.50	0.67	
UPU23	0.63	0.38	0.43	0.50	0.54	0.54	0.59	

(dissociation energies in group-1 and -2 diatomics), and PA26. It makes sense that revPBE exchange is poor for atomisation energies since, unlike most exchange functionals, it was not fit to atomic exchange energies.⁵⁹ However, revPBE0 still yields the lowest WTMAD-4 of all XDM-corrected functionals due to its excellent performance for WATER27 (binding energies of water clusters). Replacing BJ damping with Z damping slightly improves the performance for WATER27 using revPBE0, but significantly increases the overbinding seen with B86bPBE0 and LC-whPBE.

The overall WTMAD-4 values obtained for the GMTKN55 using all XDM-corrected functionals considered are summarised in

Table 3. The table also shows the distribution of MAD_i values, as indicated by selected $N_{r>h}$ and $N_{d>h}$ metrics. As expected, the GGA functionals show larger errors than the hybrid and range-separated hybrid functionals, with maximum differences from the representative means seen for the SIE4x4 set (systems with large self-interaction errors). In terms of the WTMAD-4, B86b and revPBE exchange generally outperform PBE exchange, which reinforces our previous conclusion as to the importance of using a dispersionless DFA in combination with post-SCF dispersion corrections.⁷⁴ Despite reduced self-interaction error, the 50% hybrid functionals offer overall poorer performance than the 20-25% hybrids, with the W4-11 set of atomisation energies consistently being a large outlier. Finally, the WTMAD-4's for the range-separated hybrids are quite sensitive to the choice of range-separation parameter and neglect or inclusion of short-range exact-exchange mixing. The C60ISO set is a large outlier for all the RS functionals will full long-range exact exchange.

The best performing XDM-based method overall is revPBE0-XDM(Z), which gives the lowest WTMAD-4 (5.43) and, importantly, no large outliers with errors greater than 2× the mean MAD obtained with our 10 reference DFAs ($N_{r>2} = 0$), although W4-11 remains a significant outlier in terms of absolute error (2.83 kcal/mol above the mean MAD). While revPBE0-XDM(BJ) has a similar WTMAD-4, ALK8 remains a very large outlier in terms of both relative and absolute errors. B86bPBE0-XDM(Z) the second best-performing combination overall, with a higher WTMAD-4 (5.85), but having $N_{r>2} = 0$ and also $N_{d>2} = 0$; the largest absolute error occurs for WATER27, where the MAD is 1.68 kcal/mol above the mean MAD. Thus, the choice of revPBE0-XDM(Z) versus B86bPBE0-XDM(Z) may come down to whether the user prefers greater accuracy for atomisation energies, or for water clusters, which will depend on whether they are modelling covalent or non-covalent chemistry.

Table 4 shows the top ranked DFAs available for each “rung” of Perdew’s ladder⁷⁵ according to lowest WTMAD-4 values, combining the current data with that from Ref. 43. It has been previously demonstrated that the numerical atomic orbital (NAO) basis sets used in FHI-aims give energies in good agreement with basis-set limit results using Gaussian-type orbitals (GTOs).^{76,77} Indeed, the extremely similar metrics for revPBE-D3(BJ) shown on the first two lines of Table 4 confirm that NAO and GTO results are directly comparable. However, it is notable that the tight basis set in FHI-aims includes fewer functions than the typical def2-QZVPP(D) basis used for the GMTKN55 benchmark, yet delivers nearly the same results.

From the data in Table 4, XDM-corrected functionals show consistently strong performance when paired with GGAs or GGA-based global hybrids. In terms of WTMAD-4 values, the D3(BJ), XDM(BJ), and XDM(Z) dispersion corrections all perform similarly; it is principally for metal-containing benchmarks, such as ALK8, where there are notable differences that manifest in the distribution of outliers. Each of these three dispersion corrections, paired with revPBE or revPBE0, is a top-performing functional within its class. While fitting no parameters and using only GGA ingredients in the base DFAs, revPBE0 with D3(BJ), XDM(Z), and XDM(BJ) ranks 4th through 6th in terms of lowest WTMAD-4 val-

Table 3 WTMAD-4 results, numbers of outliers, and maximum outliers, for the GMTKN55 benchmark for selected functionals and dispersion corrections. $N_{r>h}$ is the number of benchmarks that have a ratio of $\text{MAD}_i/\overline{\text{MAD}}_i^{\text{10-DFA}} > h$, where the mean MAD is the value obtained from the 10 reference DFAs used in the definition of the WTMAD-4 weights. Similarly, $N_{d>h}$ is the number of benchmarks that have the difference $\text{MAD}_i - \overline{\text{MAD}}_i^{\text{10-DFA}} > h$ kcal/mol.

Functional	XDM(BJ)								XDM(Z)									
	WTMAD-4	$N_{r<1}$	$N_{r>2}$	Max r	Set	$N_{d>2}$	$N_{d>5}$	MAX d	Set	WTMAD-4	$N_{r<1}$	$N_{r>2}$	Max r	Set	$N_{d>2}$	$N_{d>5}$	MAX d	Set
PBE	9.20	11	12	2.79	ALK8	13	8	9.86	SIE4x4	9.27	11	13	2.62	W4-11	12	7	9.96	SIE4x4
revPBE	8.45	16	7	3.76	ACONF	11	4	9.79	SIE4x4	7.91	19	7	2.51	SCONF	8	3	9.65	SIE4x4
B86bPBE	8.48	16	11	2.94	SCONF	11	4	9.80	SIE4x4	8.80	14	13	2.99	SCONF	11	4	9.82	SIE4x4
PBE0	6.21	30	1	3.19	ALK8	1	1	10.68	ALK8	6.19	28	0	1.64	WATER27	1	0	2.82	WATER27
revPBE0	5.44	42	1	2.58	ALK8	2	1	7.71	ALK8	5.43	40	0	1.48	W4-11	1	0	2.83	W4-11
B86bPBE0	5.53	39	0	1.93	ALK8	1	0	4.55	ALK8	5.85	39	0	1.55	SCONF	0	0	1.68	WATER27
B3LYP	6.27	36	2	2.44	BUT14DIOL	5	2	6.00	MB16-43	6.53	31	1	2.46	BUT14DIOL	3	1	6.88	MB16-43
PBE50	7.44	20	5	3.60	ALK8	7	5	12.67	ALK8	7.31	24	4	2.46	W4-11	6	4	8.63	W4-11
revPBE50	6.97	27	4	4.42	ALK8	8	4	16.70	ALK8	6.73	28	4	3.37	W4-11	6	4	14.02	W4-11
B86bPBE50	6.98	25	5	2.71	W4-11	7	4	10.15	W4-11	7.08	23	4	2.70	W4-11	6	4	10.05	W4-11
BHLYP	7.59	27	6	6.56	ALK8	9	5	27.14	ALK8	7.46	26	5	3.34	W4-11	9	4	18.82	MB16-43
HSE06	6.41	31	1	3.23	ALK8	1	1	10.90	ALK8	6.37	31	0	1.87	BUT14DIOL	1	0	3.75	WATER27
LC- ω PBE ^a	6.56	35	2	2.84	SCONF	5	2	5.77	SIE4x4	7.10	29	2	3.22	SCONF	6	2	5.84	SIE4x4
LC- ω PBE ^b	6.39	32	2	3.17	C60ISO	4	2	11.61	C60ISO	6.57	31	3	3.16	C60ISO	4	2	11.52	C60ISO
LC- ω hPBE ^c	5.65	42	0	2.00	ALK8	2	0	4.86	ALK8	6.09	34	0	2.00	SCONF	2	0	4.59	C60ISO
LC- ω hPBE ^d	7.10	23	4	3.73	C60ISO	7	3	14.57	C60ISO	7.23	25	4	3.73	C60ISO	8	3	14.56	C60ISO

^a $\omega = 0.2$; ^b $\omega = 0.4$; ^c $\omega = 0.2$ and $\alpha_X = 0.2$; ^d $\omega = 0.4$ and $\alpha_X = 0.2$.

ues for global hybrids. Although slightly lower WTMAD-4 values are obtained with PW6B95-D3(BJ), M052X-D3(0), and M062X-D3(0), these base functionals involve 6, 23, and 33 empirical fit parameters, respectively.⁷⁸⁻⁸⁰ They also have much more complicated functional forms, relying on high-order power-series expansions and meta-GGA ingredients that, in turn, give rise to numerical instabilities.⁸¹⁻⁸⁴ Additionally, M052X-D3(0) and M062X-D3(0) both give large outliers (for the MB16-43 and HEAVYSB11 sets, respectively), which is likely indicative of overfitting.

The analysis of outliers provides a much more nuanced assessment of the functionals than ranking by WTMAD-4 alone. The maximum difference ratios in particular show some distinct trends. For 5/6 top-ranked GGA functionals, the SIE4x4 set is the greatest outlier, as may be expected due to the inherent delocalisation error seen with this class of functional. Also, with the exception of TPSS-D3(BJ), the meta-GGAs tend to give larger outliers than the GGAs, making them difficult to recommend. Notably, the highly empirical M06L-D3(0) gives a massive error for the MB16-43 set, indicating this functional to be overfit, providing unphysical performance for a benchmark that is chemically distinct from its training data. B97-D3(BJ) also shows some evidence of overfitting, with MB16-43 again being the maximum outlier, albeit with a much lower MAD than M06L-D3(0).

Turning to the hybrid functionals, it appears that low WTMAD-4 values are often obtained at the expense of one or two benchmarks that are large outliers. This is quite evident for ω B97X-V, which gives above-average performance for 50 benchmarks, but shows a large ratio outlier for C60ISO and a large difference outlier for MB16-43. ω B97X-D3(0) also shows a large difference outlier for the mindless benchmark, again illustrating the problems with overfitting of highly empirical functionals. The C60ISO set remains a large outlier for other RS hybrids with full long-range exact exchange, which provides a poor description of large systems with highly extended conjugation and small band gaps. Correlation models with improved long-range physics are needed to pair well with exact (Hartree-Fock) exchange.⁸⁵

Of the global hybrid functionals, revPBE0-D3(BJ), revPBE0-XDM(Z), MPW1B95-D3(BJ), MPW1PW91-D3(BJ), and B86bPBE0-XDM(Z) all offer a good balance between a low

WTMAD-4 and few or no large outliers. MPW1B95-D3(BJ) involves the B95 meta-GGA correlation functional, which is known to suffer from numerical instabilities.^{81,82} However, the other four methods listed above use only GGA ingredients in their base functionals and appear to be the most consistently reliable choices. Each of the revPBE, MPW1, and B86b exchange functionals give good agreement with exact exchange repulsion in noble-gas dimers,^{59,86,87} emphasising the advantages of dispersionless exchange in functional development. We note that the pairing of MPW1PW91 with XDM(Z) was not considered in this work as that functional is not implemented in FHI-aims (except via libxc⁸⁸), but that may be a promising combination for future work.

In addition to our XDM variants, we also evaluated the performance of the TS, MBD@rsSCS, and MBD-NL dispersion corrections, all paired with PBE and PBE0. We note that MBD@rsSCS and MBD-NL failed for some systems due to a polarisation catastrophe.²¹ For MBD@rsSCS two reactions from ALK8 were substituted using MBD-NL results for each of PBE ($\text{Na}_8 \rightarrow 4\text{Na}_2$ and $\text{Li}_5\text{CH} \rightarrow \text{Li}_4\text{C} + \text{LiH}$) and PBE0 ($\text{Na}_8 \rightarrow 4\text{Na}_2$ and $(\text{Li}(\text{CH}_2)\text{N})_2 \rightarrow 2\text{Li}(\text{CH}_2)\text{N}$). Similarly for MBD-NL, the forward and reverse barrier heights for the $\text{F} + \text{H}_2 \rightarrow \text{HF} + \text{H}$ reaction from BH76 were substituted using MBD@rsSCS results for both PBE and PBE0.

Ultimately, the GMTKN55 results for TS, MBD@rsSCS, and MBD-NL did not place among the best-ranking functional-DC combinations shown in Table 4, with WTMAD-4 values of 9.85, 9.44, and 9.42 for PBE, and 6.72, 6.30, and 6.36 for PBE0, respectively. Thus, we will limit our discussion to qualitative metrics, and the full data will be provided in the ESI. The TS method shows its largest errors for isomerisation energies and large systems (iso+large) category and, for the ALK8 set, MBD@rsSCS shows similar errors to XDM(BJ). Generally, MBD-NL and XDM(Z) are more consistently accurate across all GMTKN55 categories. Inspecting the outliers shows that PBE0-MBD-NL has $N_{r>2} = N_{d>2} = 0$, while also exhibiting good performance for MB16-43 with a MAE of 14.86. However, due to the aforementioned convergence issues and very limited choice of base functionals, we do not recommend these MBD methods for general thermochemical applications to molecular systems.

Table 4 The top 6 GGAs, 4 mega-GGAs, 12 global hybrids, 6 range-separated hybrids, and 6 double-hybrid functionals according to WTMAD-4. Data compiled from the present study and Ref. 43. Also shown are the numbers of outliers and the GKMTKN55 subset responsible for the maximum outlier in terms of both percent and absolute errors.

Functional	WTMAD-4	$N_{r \leq 1}$	$N_{r > 2}$	MAX r	Set	$N_{d > 2}$	$N_{d > 5}$	MAX d	Set
revPBE-D3(BJ) ^a	7.67	16	2	2.22	BHPERI	9	2	9.70	SIE4x4
revPBE-D3(BJ) ^b	7.73	16	3	2.26	BHPERI	8	2	9.83	SIE4x4
revPBE-XDM(Z)	7.91	19	7	2.51	SCONF	8	3	9.65	SIE4x4
OLYP-D3(BJ)	8.16	18	6	2.51	BHPERI	13	2	11.95	SIE4x4
B97-D3(BJ)	8.32	19	6	2.57	AL2X6	12	4	16.80	MB16-43
revPBE-XDM(BJ)	8.45	16	7	3.76	ACONF	11	4	9.79	SIE4x4
revTPSS-D3(BJ)	7.73	23	3	3.71	SCONF	9	2	17.45	MB16-43
SCAN-D3(BJ)	7.95	20	3	3.20	ALKBDE10	10	2	13.24	ALKBDE10
TPSS-D3(BJ)	7.95	19	2	3.14	SCONF	10	3	8.31	SIE4x4
M06L-D3(0)	8.92	18	8	5.43	ADIM6	8	1	43.97	MB16-43
PW6B95-D3(BJ)	5.14	41	1	2.31	IL16	0	0	1.76	SIE4x4
M052X-D3(0)	5.19	41	1	2.08	ADIM6	3	1	7.02	MB16-43
M062X-D3(0)	5.22	46	2	3.50	HEAVYSB11	1	1	5.83	HEAVYSB11
revPBE0-D3(BJ) ^a	5.30	43	0	1.51	W4-11	1	0	3.03	W4-11
revPBE0-XDM(Z)	5.43	40	0	1.48	W4-11	1	0	2.83	W4-11
revPBE0-XDM(BJ)	5.44	42	1	2.58	ALK8	2	1	7.71	ALK8
MPW1B95-D3(BJ)	5.48	42	1	2.02	ACONF	0	0	0.85	RSE43
B86bPBE0-XDM(BJ)	5.53	39	0	1.93	ALK8	1	0	4.55	ALK8
M08HX-D3(0)	5.68	41	2	3.85	ACONF	1	0	2.26	C60ISO
MPW1PW91-D3(BJ)	5.82	32	0	1.31	PNICO23	0	0	1.04	ALK8
B86bPBE0-XDM(Z)	5.85	39	0	1.55	SCONF	0	0	1.68	WATER27
PBE0-D3(BJ) ^a	5.90	33	0	1.36	WATER27	0	0	1.60	WATER27
ω B97X-V	4.40	50	1	2.57	C60ISO	2	2	13.21	MB16-43
ω B97X-D3(0)	5.38	40	1	2.54	C60ISO	2	2	17.20	MB16-43
LC- ω hPBE-XDM(BJ) ^c	5.65	42	0	2.00	ALK8	2	0	4.86	ALK8
HSE06-D3(BJ)	6.08	32	0	1.43	PCONF21	0	0	1.85	WATER27
LC- ω hPBE-XDM(Z) ^d	6.09	34	0	2.00	SCONF	2	0	4.59	C60ISO
LC- ω PBE-XDM(BJ) ^e	6.39	32	2	3.17	C60ISO	4	2	11.61	C60ISO
DH24	2.23	52	0	1.57	C60ISO	1	0	3.07	C60ISO
revDH23	2.26	52	0	1.56	C60ISO	1	0	2.99	C60ISO
SOS-DH24	2.27	52	0	1.26	IL16	0	0	0.66	C60ISO
SOS-DH23	2.34	52	0	1.35	IL16	0	0	0.73	C60ISO
ω DOD-PBEP86-D3(BJ) ^f	2.50	53	0	1.35	ADIM6	0	0	0.73	DIPCS10
ω DOD-PBEP86-D3(BJ) ^g	2.52	53	0	1.54	ADIM6	0	0	0.30	DIPCS10

^aPresent work; ^bliterature data; ^c $\omega = 0.2$, $a_X = 0.2$; ^d $\omega = 0.2$, $a_X = 0.2$; ^e $\omega = 0.4$; ^f $\omega = 0.10$, $a_X = 0.69$; ^g $\omega = 0.08$, $a_X = 0.72$

5.2 Molecular-Crystal Benchmarks

While XDM(Z) appears consistently reliable across the GMTKN55, it is also crucial to examine its performance in the solid state. Therefore, we consider the absolute lattice energies of the X23, HalCrys4, and ICE13 data sets, as well as the relative lattice energies of ICE13. Tabulated results for XDM(BJ) and XDM(Z) using the basis-set correction of Eq. 11 are presented in Table 5.

The results in Table 5 show that the GGA functionals perform reasonably well, except for HalCrys4, where they overbind substantially due to delocalisation error. Similar overbinding is also for ICE13-Abs with XDM-corrected PBE and B86bPBE, but not revPBE, indicating an interplay between delocalisation error and the exchange enhancement factor. While anomalous for GGAs, the excellent performance of dispersion-corrected revPBE for both ICE13 benchmarks has been noted previously, leading to its popularity for simulations of water and ice.^{49,89} With the single exception of revPBE for ICE13-Abs, the 25% hybrid functionals perform significantly better than their GGA counterparts, while fur-

ther increases in exact-exchange mixing result in larger errors in most cases. Which of XDM(BJ) versus XDM(Z) is more accurate is highly dependent on both the benchmark and base functional. Nonetheless, XDM(Z) provides consistently good performance when paired with any of PBE0, revPBE0, or B86bPBE0.

Only large-basis results have been considered in the above discussion to avoid confounding variables such as error cancellation. However, as shown in the ESI, the various methods also perform with exceptional accuracy and consistency for the molecular crystal benchmarks with the `lightdenser` basis setting, rivalling or even exceeding the basis-set-corrected results in Table 5. This performance is worth noting, as these benchmarks are indicative of a method's effectiveness for crystal structure prediction (CSP). In CSP workflows, basis-set corrections are often used only for final energy refinement due to time and computational constraints; in practice, geometry optimisations and preliminary energy ranking typically employ a smaller basis such as `lightdenser`.

Table 5 Mean absolute errors, in kcal/mol, for the X23, HalCrys4, and ICE13 (absolute and relative) lattice-energy benchmarks. All results are shown for tight basis settings at lightdenser geometries; for the hybrid functionals, this involved the basis-set correction of Eq. 11.

Functional	X23		HalCrys4		ICE13-Abs		ICE13-Rel	
	BJ	Z	BJ	Z	BJ	Z	BJ	Z
PBE	1.31	0.92	5.49	4.12	1.44	2.10	0.82	0.61
revPBE	1.27	1.30	3.55	4.69	0.30	0.30	0.39	0.30
B86bPBE	0.70	0.81	4.70	5.03	1.56	1.88	0.52	0.41
PBE0	1.00	0.66	1.61	0.57	0.43	0.50	0.48	0.29
revPBE0	0.90	0.71	2.47	1.12	1.36	0.79	0.23	0.21
B86bPBE0	0.48	0.61	1.21	0.86	0.30	0.36	0.31	0.17
PBE50	0.87	0.75	1.78	3.78	1.30	0.69	0.21	0.24
revPBE50	0.72	0.74	2.81	3.71	2.18	1.41	0.18	0.39
B86bPBE50	0.51	0.73	1.10	3.36	1.25	0.73	0.18	0.33

6 Summary

This work considers a new variant of the XDM dispersion model that addresses previous overbinding of metal clusters. It is the first study to test the XDM (and MBD) methods for the GMTKN55 data set, enabling a direct, head-to-head comparison of the most widely used dispersion corrections on a comprehensive benchmark for general main-group thermochemistry, kinetics, and non-covalent interactions. The canonical XDM(BJ) method showed strong results in all cases with the exception of the ALK8 benchmark, which originally motivated the study into Z damping. XDM(Z) completely resolved this error and, despite eliminating one empirical parameter, still performs on par with other leading dispersion corrections for the GMTKN55 set. We therefore recommend XDM(Z) as a good general method for both molecular and solid-state applications due to its overall reliability.

Overall, MPW1PW91-D3(BJ), B86bPBE0-XDM(Z), revPBE0-D3(BJ), and revPBE0-XDM(Z) are the best exchange-correlation functionals among those tested. Despite their simplicity, they give WTMAD-4 values only slightly higher than the best hybrid functionals available in the literature,^{38,72} but with minimal outliers. revPBE0-XDM(Z) and revPBE0-D3(BJ) are particularly accurate for water clusters, while B86bPBE0-XDM(Z) and MPW1PW91-D3(BJ) are more accurate for atomisation energies. Any of these four methods is an excellent choice for a simple, minimally empirical density functional. For molecular crystals, XDM(Z) paired with any of PBE0, revPBE0, and B86bPBE0 demonstrates consistent accuracy. Thus, revPBE0-XDM(Z) and B86bPBE0-XDM(Z) emerge as reliable, minimally empirical methods that perform consistently well across molecular chemistry.

Finally, analysis of the outliers (as opposite to only weighted mean absolute errors) was found to be particularly informative, and reveals weaknesses in particular DFAs that are not evident from their low WTMAD-4 values. It can be argued that introducing improved physics to eliminate the largest outliers is a better general strategy for ongoing functional development than introducing increasing numbers of empirical parameters to achieve slightly better across-the-board performance, which often comes at the expense of one or two larger outliers.

Acknowledgements

KRB and ERJ thank the Natural Sciences and Engineering Research Council (NSERC) of Canada for financial support and the Atlantic Computing Excellence Network (ACENET) for computational resources. ERJ additionally thanks the Royal Society for a Wolfson Visiting Fellowship, while KRB thanks the Killam Trust, the Government of Nova Scotia, and the Mary Margaret Werner Graduate Scholarship Fund.

Data Availability Statement

The data that support the findings of this study are available in the supplementary information.

Conflicts of Interest

There are no conflicts to report.

References

- 1 M. Dion, H. Rydberg, E. Schröder, D. C. Langreth and B. I. Lundqvist, *Phys. Rev. Lett.*, 2004, **92**, 246401.
- 2 G. Román-Pérez and J. M. Soler, *Phys. Rev. Lett.*, 2009, **103**, 096102.
- 3 K. Lee, É. D. Murray, L. Kong, B. I. Lundqvist and D. C. Langreth, *Phys. Rev. B*, 2010, **82**, 081101.
- 4 O. A. Vydrov and T. Van Voorhis, *J. Chem. Phys.*, 2010, **133**, 244103.
- 5 R. Sabatini, T. Gorni and S. De Gironcoli, *Phys. Rev. B*, 2013, **87**, 041108.
- 6 S. Grimme, *J. Comput. Chem.*, 2004, **25**, 1463–1473.
- 7 S. Grimme, *J. Comput. Chem.*, 2006, **27**, 1787–1799.
- 8 S. Grimme, J. Antony, S. Ehrlich and H. Krieg, *J. Chem. Phys.*, 2010, **132**, 154104.
- 9 S. Grimme, S. Ehrlich and L. Goerigk, *J. Comput. Chem.*, 2011, **32**, 1456–1465.
- 10 E. Caldeweyher, S. Ehlert, A. Hansen, H. Neugebauer, S. Spicher, C. Bannwarth and S. Grimme, *J. Chem. Phys.*, 2019, **150**, 154122.
- 11 A. Tkatchenko and M. Scheffler, *Phys. Rev. Lett.*, 2009, **102**, 073005.
- 12 A. Tkatchenko, R. A. DiStasio Jr, R. Car and M. Scheffler, *Phys. Rev. Lett.*, 2012, **108**, 236402.

13 A. Ambrosetti, A. M. Reilly, R. A. DiStasio Jr and A. Tkatchenko, *J. Chem. Phys.*, 2014, **140**, 18A508.

14 J. Hermann and A. Tkatchenko, *Phys. Rev. Lett.*, 2020, **124**, 146401.

15 M. Kim, W. J. Kim, T. Gould, E. K. Lee, S. Lebegue and H. Kim, *J. Am. Chem. Soc.*, 2020, **142**, 2346–2354.

16 T. Gould, S. Lebegue, J. G. Ángyán and B. Tomáš, *J. Chem. Theory Comput.*, 2016, **12**, 5920–5930.

17 E. R. Johnson, in *The Exchange-Hole Dipole Moment Dispersion Model*, Elsevier, 2017, ch. 5, pp. 169–194.

18 A. D. Becke and E. R. Johnson, *J. Chem. Phys.*, 2005, **123**, 154101.

19 E. R. Johnson and A. D. Becke, *J. Chem. Phys.*, 2006, **124**, 174104.

20 A. D. Becke and E. R. Johnson, *J. Chem. Phys.*, 2007, **127**, 154108.

21 K. R. Bryenton and E. R. Johnson, *J. Chem. Phys.*, 2023, **158**, 204110.

22 K. R. Bryenton, *Oscallot*, 2023, <https://doi.org/10.5281/zenodo.7942358>.

23 A. Otero-de-la Roza and E. R. Johnson, *J. Chem. Phys.*, 2013, **138**, 204109.

24 C. J. Nickerson, K. R. Bryenton, A. J. Price and E. R. Johnson, *J. Phys. Chem. A*, 2023, **127**, 8712–8722.

25 A. A. Adeleke and E. R. Johnson, *Phys. Rev. B*, 2023, **107**, 064101.

26 A. Otero-de-la Roza and E. R. Johnson, *J. Chem. Phys.*, 2020, **153**, 054121.

27 M. S. Christian, E. R. Johnson and T. M. Besmann, *J. Phys. Chem. A*, 2021, **125**, 2791–2799.

28 A. Otero-de-la Roza, L. M. LeBlanc and E. R. Johnson, *J. Phys. Chem. Lett.*, 2020, **11**, 2298–2302.

29 M. S. Christian, A. Otero-de-la Roza and E. R. Johnson, *J. Chem. Theory Comput.*, 2016, **12**, 3305–3315.

30 M. S. Christian, A. Otero-de-la Roza and E. R. Johnson, *Carbon*, 2017, **124**, 531–540.

31 A. Otero-de-la Roza and E. R. Johnson, *J. Chem. Phys.*, 2012, **137**, 054103.

32 A. Otero-de-la Roza, B. H. Cao, I. K. Price, J. E. Hein and E. R. Johnson, *Angew. Chem. Int. Ed.*, 2014, **53**, 7879–7882.

33 V. Blum, R. Gehrke, F. Hanke, P. Havu, V. Havu, X. Ren, K. Reuter and M. Scheffler, *Comput. Phys. Commun.*, 2009, **180**, 2175–2196.

34 A. J. A. Price, A. Otero-de-la-Roza and E. R. Johnson, *Chem. Sci.*, 2023, **14**, 1252–1262.

35 A. J. A. Price, R. A. Mayo, A. Otero-de-la-Roza and E. R. Johnson, *CrystEngComm*, 2023, **25**, 953–960.

36 R. A. Mayo, A. J. A. Price, A. Otero-de-la-Roza and E. R. Johnson, *Acta Crystallogr.*, 2024, **B80**, 595–605.

37 A. D. Becke, *J. Chem. Phys.*, 2024, **160**, 204118.

38 L. Goerigk, A. Hansen, C. Bauer, S. Ehrlich, A. Najibi and S. Grimme, *Phys. Chem. Chem. Phys.*, 2017, **19**, 32184–32215.

39 A. Otero-de-la-Roza, K. R. Bryenton, F. Kannemann, E. R. Johnson, R. M. Dickson, H. Schmider and A. D. Becke, *postg (release: XCDM(Z))*, 2015, <https://github.com/aterodelaroza/postg>.

40 F. O. Kannemann and A. D. Becke, *J. Chem. Theory Comput.*, 2010, **6**, 1081–1088.

41 A. Otero-de-la-Roza, *refdata*, 2015, <https://github.com/aterodelaroza/refdata>.

42 E. R. Johnson, *gmtkn55-fhiaims*, 2024, <https://github.com/erin-r-johnson/gmtkn55-fhiaims>.

43 K. R. Bryenton and E. R. Johnson, *Phys. Chem. Chem. Phys.*, 2026, **28**, 1463–1469.

44 A. M. Reilly and A. Tkatchenko, *J. Chem. Phys.*, 2013, **139**, 024705.

45 G. A. Dolgonos, J. Hoja and A. D. Boese, *Phys. Chem. Chem. Phys.*, 2019, **21**, 24333–24344.

46 A. Otero-de-la Roza, L. M. LeBlanc and E. R. Johnson, *J. Chem. Theory Comput.*, 2019, **15**, 4933–4944.

47 J. A. Dean, *Lange's Handbook of Chemistry*, McGraw-Hill, 15th edn., 1999.

48 J. G. Brandenburg, T. Maas and S. Grimme, *J. Chem. Phys.*, 2015, **142**, 124104.

49 F. Della Pia, A. Zen, D. Alfè and A. Michaelides, *J. Chem. Phys.*, 2022, **157**, 134701.

50 X. Ren, P. Rinke, V. Blum, J. Wieferink, A. Tkatchenko, A. Sanfilippo, K. Reuter and M. Scheffler, *New J. Phys.*, 2012, **14**, 053020.

51 S. V. Levchenko, X. Ren, J. Wieferink, R. Johann, P. Rinke, V. Blum and M. Scheffler, *Comput. Phys. Commun.*, 2015, **192**, 60–69.

52 S. Kokott, F. Merz, Y. Yao, C. Carbogno, M. Rossi, V. Havu, M. Rampp, M. Scheffler and V. Blum, *J. Chem. Phys.*, 2024, **161**, 024112.

53 V. W.-z. Yu, F. Corsetti, A. García, W. P. Huhn, M. Jacquelin, W. Jia, B. Lange, L. Lin, J. Lu, W. Mi, A. Seifitokaldani, A. Vázquez-Mayagoitia, C. Yang, H. Yang and V. Blum, *Comput. Phys. Commun.*, 2018, **222**, 267–285.

54 V. Havu, V. Blum, P. Havu and M. Scheffler, *J. Chem. Phys.*, 2009, **228**, 8367–8379.

55 A. C. Ihrig, J. Wieferink, I. Y. Zhang, M. Ropo, X. Ren, P. Rinke, M. Scheffler and V. Blum, *New J. Phys.*, 2015, **17**, 093020.

56 A. D. Becke, *J. Chem. Phys.*, 1986, **84**, 4524–4529.

57 J. P. Perdew, K. Burke and M. Ernzerhof, *Phys. Rev. Lett.*, 1996, **77**, 3865.

58 J. P. Perdew, K. Burke and M. Ernzerhof, *Phys. Rev. Lett.*, 1997, **78**, 1396–1396.

59 Y. Zhang and W. Yang, *Phys. Rev. Lett.*, 1998, **80**, 890–890.

60 A. D. Becke, *J. Chem. Phys.*, 1986, **85**, 7184–7187.

61 A. D. Becke, *Phys. Rev. A*, 1988, **38**, 3098.

62 A. D. Becke, *J. Chem. Phys.*, 1993, **98**, 5648–5652.

63 C. Lee, W. Yang and R. G. Parr, *Phys. Rev. B*, 1988, **37**, 785.

64 P. J. Stephens, F. J. Devlin, C. F. Chabalowski and M. J. Frisch, *J. Phys. Chem.*, 1994, **98**, 11623–11627.

65 S. H. Vosko, L. Wilk and M. Nusair, *Can. J. Phys.*, 1980, **58**,

1200–1211.

66 C. Adamo and V. Barone, *J. Chem. Phys.*, 1999, **110**, 6158–6170.

67 A. D. Becke, *J. Chem. Phys.*, 1993, **98**, 1372–1377.

68 K. R. Bryenton, A. A. Adeleke, S. G. Dale and E. R. Johnson, *WIREs: Comput. Mol. Sci.*, 2023, **13**, e1631.

69 A. V. Kruckau, O. A. Vydrov, A. F. Izmaylov and G. E. Scuseria, *J. Chem. Phys.*, 2006, **125**, 224106.

70 O. A. Vydrov and G. E. Scuseria, *J. Chem. Phys.*, 2006, **125**, 234109.

71 O. A. Vydrov, G. E. Scuseria and J. P. Perdew, *J. Chem. Phys.*, 2007, **126**, 154109.

72 G. Santra, N. Sylvestry and J. M. Martin, *J. Phys. Chem. A*, 2019, **123**, 5129–5143.

73 J. Hoja and A. Tkatchenko, *Faraday Discuss.*, 2018, **211**, 253–274.

74 A. J. A. Price, K. R. Bryenton and E. R. Johnson, *J. Chem. Phys.*, 2021, **154**, 230902.

75 J. P. Perdew and K. Schmidt, AIP Conf. Proc., 2001, pp. 1–20.

76 J. W. Abbott, C. M. Acosta, A. Akkoush, A. Ambrosetti, V. Atalla, A. Bagrets, J. Behler, D. Berger, B. Bieniek, J. Björk, V. Blum, S. Bohloul, C. L. Box, N. Boyer, D. S. Brambila, G. A. Bramley, K. R. Bryenton, M. Camarasa-Gómez, C. Carbogno, F. Caruso, S. Chutia, M. Ceriotti, G. Csányi, W. Dawson, F. A. Delesma, F. D. Sala, B. Delley, R. A. D. Jr., M. Dragomir, S. Driessens, M. Dvorak, S. Erker, F. Evers, E. Fabiano, M. R. Farrow, F. Fiebig, J. Filser, L. Foppa, L. Gallandi, A. Garcia, R. Gehrke, S. Ghan, L. M. Ghiringhelli, M. Glass, S. Goedecker, D. Golze, J. A. Green, A. Grisafi, A. Grüneis, J. Günzl, S. Gutzeit, S. J. Hall, F. Hanke, V. Havu, X. He, J. Hekele, O. Hellman, U. Herath, J. Hermann, D. Hernangómez-Pérez, O. T. Hofmann, J. Hoja, S. Hollweger, L. Hörmann, B. Hourahine, W. B. How, W. P. Huhn, M. Hülsberg, S. P. Jand, H. Jiang, E. R. Johnson, W. Jürgens, J. M. Kahk, Y. Kanai, K. Kang, P. Karpov, E. Keller, R. Kempt, D. Khan, M. Kick, B. P. Klein, J. Kloppenburg, A. Knoll, F. Knoop, F. Knuth, S. S. Köcher, J. Kockläuner, S. Kokott, T. Körzdörfer, H.-H. Kowalski, P. Kratzer, P. Kus, R. Laasner, B. Lang, B. Lange, M. F. Langer, A. H. Larsen, H. Lederer, S. Lehtola, M.-O. Lenz-Himmer, M. Leucke, S. Levchenko, A. Lewis, O. A. von Lilienfeld, K. Lion, W. Lipsunen, J. Lischner, Y. Litman, C. Liu, Q.-L. Liu, A. J. Logsdail, M. Lorke, Z. Lou, I. Mandzhieva, A. Marek, J. T. Margraf, R. J. Mauer, T. Melson, F. Merz, J. Meyer, G. S. Michelitsch, T. Mizoguchi, E. Moerman, D. Morgan, J. Morgenstern, J. Moussa, A. S. Nair, L. Nemeć, H. Oberhofer, A. O. de-la Roza, R. L. Panadés-Barrueta, T. Patlolla, M. Pogodaeva, A. Pöppl, A. J. A. Price, T. A. R. Purcell, J. Quan, N. Raimbault, M. Rampp, K. Rasim, R. Redmer, X. Ren, K. Reuter, N. A. Richter, S. Ringe, P. Rinke, S. P. Rittmeyer, H. I. Rivera-Arrieta, M. Ropo, M. Rossi, V. Ruiz, N. Rybin, A. Sanfilippo, M. Scheffler, C. Scheurer, C. Schober, F. Schubert, T. Shen, C. Shepard, H. Shang, K. Shibata, A. Sobolev, R. Song, A. Soon, D. T. Speckhard, P. V. Stishenko, M. Tahir, I. Takahara, J. Tang, Z. Tang, T. Theis, F. Theiss, A. Tkatchenko, M. Todorović, G. Trenins, O. T. Unke, Álvaro Vázquez-Mayagoitia, O. van Vuren, D. Waldschmidt, H. Wang, Y. Wang, J. Wieferink, J. Wilhelm, S. Woodley, J. Xu, Y. Xu, Y. Yao, Y. Yao, M. Yoon, V. W. zhe Yu, Z. Yuan, M. Zacharias, I. Y. Zhang, M.-Y. Zhang, W. Zhang, R. Zhao, S. Zhao, R. Zhou, Y. Zhou and T. Zhu, *arXiv preprint arXiv:2505.00125*, 2025.

77 S. R. Jensen, S. Saha, J. A. Flores-Livas, W. Huhn, V. Blum, S. Goedecker and L. Frediani, *J. Phys. Chem. Lett.*, 2017, **8**, 1449–1457.

78 Y. Zhao and D. G. Truhlar, *J. Phys. Chem. A*, 2005, **109**, 5656–5667.

79 Y. Zhao, N. E. Schultz and D. G. Truhlar, *J. Chem. Theory Comput.*, 2006, **2**, 364–382.

80 Y. Zhao and D. G. Truhlar, *Theor. Chem. Acc.*, 2008, **120**, 215–241.

81 E. R. Johnson, R. A. Wolkow and G. A. DiLabio, *Chem. Phys. Lett.*, 2004, **394**, 334–338.

82 E. R. Johnson, A. D. Becke, C. D. Sherrill and G. A. DiLabio, *J. Chem. Phys.*, 2009, **131**, 034111.

83 S. E. Wheeler and K. N. Houk, *J. Chem. Theory Comput.*, 2010, **6**, 395–404.

84 N. Mardirossian and M. Head-Gordon, *J. Chem. Theory Comput.*, 2016, **12**, 4303–4325.

85 A. D. Becke, *J. Chem. Phys.*, 2003, **119**, 2972–2977.

86 C. Adamo and V. Barone, *J. Chem. Phys.*, 1998, **108**, 664–675.

87 Y. Zhang, W. Pan and W. Yang, *J. Chem. Phys.*, 1997, **107**, 7921–7925.

88 S. Lehtola, C. Steigemann, M. J. Oliveira and M. A. Marques, *SoftwareX*, 2018, **7**, 1–5.

89 V. Kapil, C. Schran, A. Zen, J. Chen, C. J. Pickard and A. Michaelides, *Nature*, 2022, **609**, 512–516.